Check for updates

Water-soluble gold nanoparticles: recyclable catalysts for the reduction of aromatic nitro compounds in water

Gustavo A. Monti,[ab] N. Mariano Correa, [iD] [ab] R. Darío Falcone, [iD] [ab]
Gustavo F. Silbestri [iD] *[c] and Fernando Moyano [iD] *[ab]

A structure/catalytic activity study of water-soluble gold nanoparticles, stabilized by zwitterionic ligands derived from imidazolium salts, in the reduction of aromatic nitro compounds in pure water at different temperature, as well as their recyclability, was performed. Our studies indicate that the nanoparticles synthesized by an easy, fast and reproducible process, need a short characteristic induction time to restructure the surfaces and make them active. The differences observed in the catalytic activity of the nanoparticles, determined by using the typical Langmuir–Hinshelwood model, are strongly based on the degree of coverage and spatial arrangement of the imidazolium salts on them. Finally, we demonstrate that gold nanoparticles stabilized by non-traditional ligands can be an excellent choice for nitro compound degradation.

Introduction

In recent years, many books and reviews about the application of gold in homogeneous catalysis have appeared. Normally, Au^{1+} or Au^{3+} organic complexes are used as catalysts.[1,2] However, recently, Wang *et al.*[3] conducted a detailed review of the synthetic methods and functional properties of various nanostructured materials of noble metals (especially Au and Ag). Also, they present and discuss the applications of nanomaterials for chemical systems and biosensors. The interest in metallic nanoparticles (M–NPs) has increased due to their numerous applications such as in medicine,[4,5] optics,[6,7] electronics,[8] luminescence[9] and especially because of their potential use in catalysis.[10–12]

It is well known that, when the size of a system is reduced to the nanometer scale, matter exhibits some specific properties that may be significantly different from the physical properties of the massive material. These properties depend on several factors, such as the shape, size and functionalization of the surface of the NPs and, they can be adapted if you have control over the morphology and size of the system, which can be achieved by manipulating the synthesis conditions of the NPs.

In the field of catalysis, one of the fasted growing areas in nanoscience, different stabilizers not only avoid the undesired aggregation and coalescence but can act as active spectators that may attend the catalytic properties of the metal.[13,14] At the same time, the stabilization of M–NPs by the coordinating capping ligands, results in a change of the surface properties and the surface accessibility of the nanoparticles particularly with regard to applications in catalysis.[15] Catalysis by transition-metal NPs dispersal in water allows the development of synthesis procedures with low environmental impact, easy catalyst recycling, and separation from products.[16,17]

It is known that, due to their high surface energy, M–NPs tend to aggregate. To avoid it, ligands such as thiols, amines, disulfures, thioethers, phosphines, *N*-heterocyclic carbenes (NHCs) or imidazolium salts are uses.[3] An alternative way for stabilizing metal nanoparticles can be the use of ionic liquids (ILs); the well-established and probably most studied ILs contain an imidazolium cation (*e.g.* 1-ethyl-3-methylimidazolium or 1-butyl-3-methylimidazolium) and weakly-coordinating anions such as tetrafluoroborate $[BF_4]^-$, hexafluorophosphate $[PF_6]^-$ and trifluoromethylsulfonate(triflate) $[OTf]^-$ or bis(trifluoromethylsulfonyl)imide(triflimide) $[NTf_2]^-$.[18] NHCs have been used to synthesize Au-[19,20] and Ag–NPs[21] as a model synthesis for the formation of either conglomerates or 3D networks. Glorius and co-worked described the synthesis and catalytic activity of Au- and Pd–NPs stabilized with NHCs bearing sulfonate and carboxylate groups.[22] Also, de Jesús and Chaudret have prepared, by thermal decomposition, Pt–NPs using sulfonated NHC as stabilized ligands.[23] On the other hand, Nome *et al.* have prepared Pd–NPs, water-soluble, using imidazolium-based surfactant 3-(1-

aInstituto para el desarrollo agroindustrial y de la salud, IDAS, (CONICET – UNRC), Argentina

bDepartamento de Química, Universidad Nacional de Río Cuarto, Agencia Postal # 3., Río Cuarto, C.P. X5804BYA, Argentina. E-mail: fmoyano@exa.unrc.edu.ar

cInstituto de Química del Sur (INQUISUR), Departamento de Química, Universidad Nacional del Sur (UNS), CONICET, Av. Alem 1253, B8000CPB, Bahía Blanca, Argentina. E-mail: gsilbestri@uns.edu.ar

dodecyl-3-imidazole)propanesulfonate. The NPs were effective and recycling in the aqueous biphasic hydrogenation of cyclohexene[24] and, recently we have reported the synthesis, electrostatic stabilization and characterization of Au–NPs in aqueous medium using sulfonated-imidazolium salts as stabilized.[25,26] However, these stabilizer systems may impede the activity of the M–NPs for a given reaction. At this point, a model reaction that is well known and, without the generation of by products, would be of great help.[27] Pal[28] and Esumi[29] were the first to identify the catalytic reduction of *p*-nitrophenol,[30] is perhaps the most used reaction, to test the catalytic activity of M–NPs in aqueous solution.

Continuing with our research on water-soluble gold–NPs, herein we report the structure/catalytic activity study of Au–NPs stabilized with different imidazolium salts (**1–3**, Scheme 1) in the reduction of aromatic nitro compounds in aqueous medium as well as their recyclability. Kinetic data have been obtained between 25 °C and 45 °C by monitoring the concentrations of 1,4-dinitrobenzene (DNB) by UV-vis spectroscopy and, the kinetic were modeled in terms of the Langmuir–Hinshelwood model.[31]

Results and discussion

The reaction between DNB and Hz was explored in the absence of Au–NPs and under this experimental condition no catalytic activity was observed (absorption spectra for 30 min remains unchanged). However, in the presence of catalysts, we observe changes in the spectra indicating that the reduction reaction takes place. Fig. 1 shows typical absorption spectra for the reduction reaction at different times in water, catalyzed by different Au–NPs (**1–3**) at 25 °C. It can be seen an increase in the absorbance value at $\lambda_{max} = 380$ nm with time, corresponding to the product reactions absorbance (*p*-NA) and, a decrease in the absorbance value at $\lambda_{max} = 284$ nm corresponding to the reactive (DNB) consumption. Also, it can be observed a clear isosbestic point at $\lambda_{max} = 304$ nm. This evidences the lack of

intermediates and/or product decomposition. In all cases, we observed that the reaction was completed after 30 min.

Fig. 2 shows a graph of $\ln\left(\dfrac{A_{DNB}}{A_{DNB}^0}\right)$ *versus* time (*t*) for typical reaction between DNB and Hz, catalyzed by Au–NPs. As it can be observed, the graph denotes two profiles. In the first part (red dots), it can be seen that there is an induction time (t_0), in which no reductions take places. In the second part (black dots), the reaction follows a first-order rate law. This behavior was also observed in the catalytic reduction of different substrates with metal nano-catalysts.[32,33] For example, during the catalytic reduction of *p*-nitrophenol in the presence of different catalysts, an induction period has been observed by many groups which can be as long as several minutes.[32,33] This period is usually ascribed to the diffusion time required for *p*-nitrophenol to be adsorbed onto de catalyst's surface before the reaction could start.[12,34] On the other hand, the induction time can be assigned to a surface restructuring necessary to render the M–NPs as an active catalyst[35] or, also it may be the time necessary to remove surface oxides.[36] All data published so far by different groups show that the reduction of nitrophenol proceeds on the surface of the M–NPs and quantitative analysis of this surface reaction can be performed.[31,35] Since our data indicate that the reductions begin after t_0, we determine all k_{app} values in the presence of different Au–NPs as shown in Fig. 2.

Following eqn (6), the *k* values can be determined by varying k_{app} with DNB concentrations. Fig. 3 shows the experimental data of k_{app} at different DNB concentrations in the presence of different Au–NPs (**1–3**). In all case, the profiles show an increase of k_{app} values when DNB concentration increases, which is typically due to a Langmuir–Hinshelwood mechanism.[31] These profiles clearly indicate that the catalysis process involving Au–NPs is a superficial process, where the reagents compete for the free regions on the Au–NPs surface, so that, when DNB concentrations increase, more DNB molecules are adsorbed on the catalyst and the k_{app} values increases.

The adjustments obtained with the mechanism are consistent with Wunder *et al.*[37] and *k* values were obtained by
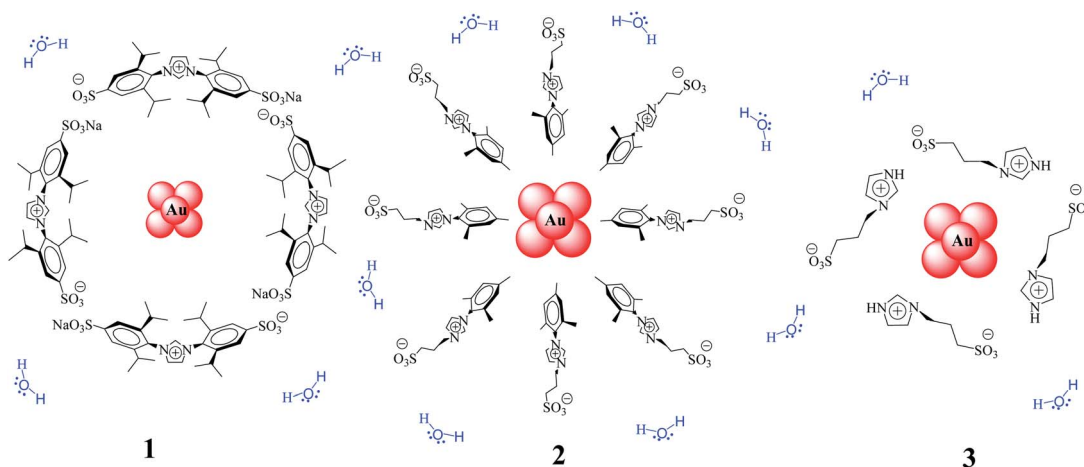
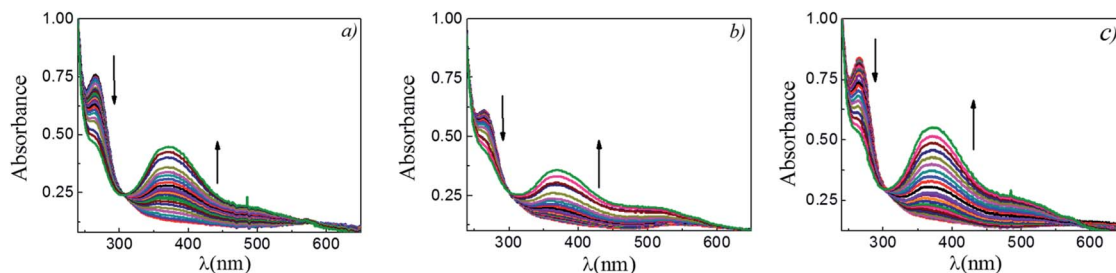**Scheme 1** Au–NPs surfaces with different sulfonated-imidazolium salts.

Fig. 1 Representative absorption spectra at different time for the reductions reactions of DNB catalyzed by different Au–NPs: (a) **1**, (b) **2** and, (c) **3**. [DNB] = 5×10^{-5} M, [Hz] = 0.1 M and, [Au–NPs] = 1×10^{-8} M.
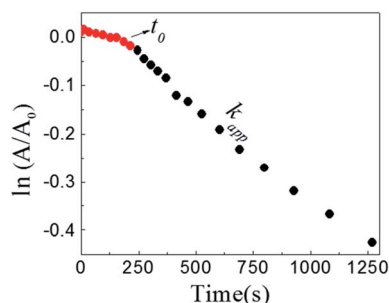

Fig. 2 Typical time trace of the absorption of the DNB at $\lambda_{max} = 284$ nm: (●) induction time, t_0; (●) section from which k_{app} is taken. [DNB] = 5×10^{-5}M, [Hz] = 0.1 M and [Au–NPs] = 1×10^{-8} M.

adjusting the experimental data to eqn (6) and, assuming $n = 0.6$ for the adsorption of DNB, while $m = 1$ for the adsorption of Hz. These values were calculated previously[37] following Gaussian distributions. The k values obtained at 25 °C for **1**, **2** and **3** are 1.03×10^{-3} mol m^2 s^{-1}, 4.07×10^{-4} mol m^2 s^{-1} and 3.10×10^{-3} mol m^2 s^{-1}, respectively. An interesting analysis arises when comparing the k of Au–NPs of similar shape and size (**2** and **3**) with the degree of coverage and spatial arrangement.[38] For **2**, there are more molecules of imidazolium salts that cover the Au–NPs and it is due to a better compaction around them.[26] This makes it difficult to approach the Au–NP surface of the reagents. Nevertheless **3** have a different arrangement around Au–NPs and then it is less compacted to **2**; the reagents can easily access the surface of Au–NPs therefore, a higher value k is observed. In other words, both the spatial arrangement and the degree of coverage are responsible for that the **3** show greater efficient catalytic in the model reaction at 25 °C.

Dependence of the reaction rate with temperature

To explain thermodynamically the k values obtained for Au–NPs, we select those Au–NPs that have a similar size (**2** and **3**, see Table 2) and; we evaluate the behavior of catalysts against the temperature in the reaction. Fig. 4 shows the k_{app} values as a function of the concentrations DNB at different temperatures for **2** and **3**, respectively.

As expected, the k_{app} values increase with temperature according to the Langmuir–Hinshelwood mechanism, which was used to determine the values of k at different temperatures as described above. Thus, it is possible to express the dependence k with temperature in terms of the Arrhenius equation.[35]

$$k = k_0 e^{-\frac{E_a}{RT}} \quad (1)$$

It is an equation that fits experimental data in most of the situations, where k_0 is the frequency factor of the surface reaction and, E_a the true activation energy which we measure in kJ mol^{-1}. Taking the natural logarithm of eqn (1), the Arrhenius equation can be rearranged as:

$$\ln k = \ln k_0 - \frac{E_a}{RT} \quad (2)$$

Fig. 5 shows the dependence k with temperature in terms of the Arrhenius linear equation to different Au–NPs (**2** and **3**).
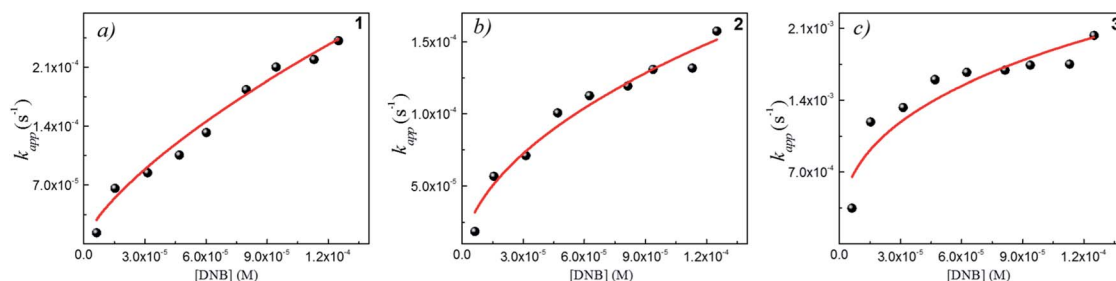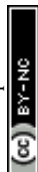

Fig. 3 Dependence of k_{app} with the DNB concentration at $T = 25$ °C for each Au–NPs: (a) **1**, (b) **2** and (c) **3**. The red lines adapt to the Langmuir–Hinshelwood model according to eqn (6). The k value was obtained considering the total surface area calculate of the catalyst for each NPs, see Table 2.
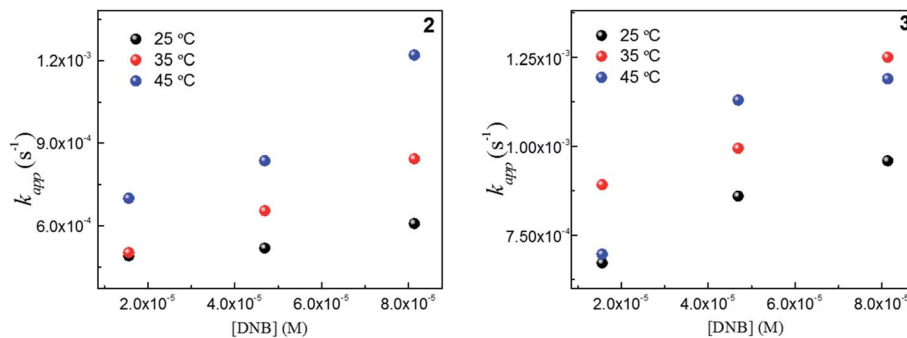
Fig. 4 Dependence of k_{app} with the DNB concentration at different temperature: (●) 25 °C, (●) 35 °C and, (●) 45 °C for 2 and 3.
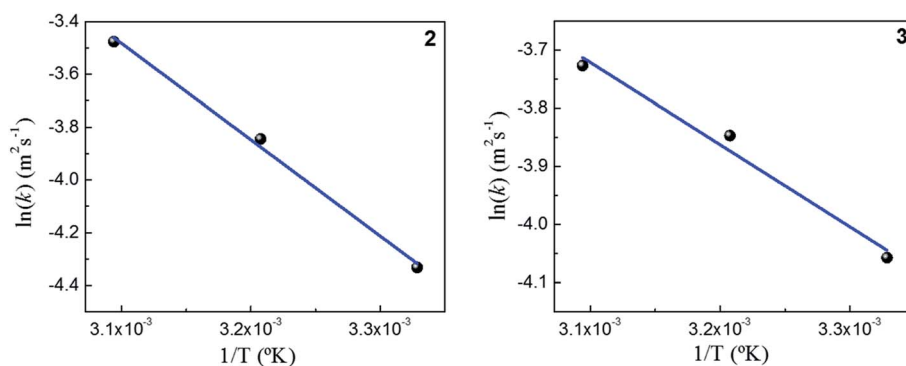

Fig. 5 Arrhenius analysis of the k obtained at different temperatures using two Au–NPs: 2 and 3.

The activation energies values found for the reaction catalyzed by 2 and 3 are 34 kJ mol^{-1} and 13 kJ mol^{-1}, respectively. Our results, shows that the lowest value of the activation energy determined corresponds with highest the value k. Furthermore, a similar value of the activation energies in metallic nanoparticles was assigned to spontaneous surface reconstruction in the absence of a substrate. In this work during the catalytic reduction of p-nitrophenol, the t_0 found for each kinetics and the activation energies determined, may indicate that there is restructuring on surfaces of Au–NPs to use as an active catalyst. It is necessary remark that the value of activation energies found to different nanocatalysts[39] varies in the range from 10 to 60 kJ mol^{-1}. Even more, these findings are similar to those Ballauff et al.[37] were the Au–NPs are immobilized on cationic

spherical polyelectrolyte brushes that ensure their stability against aggregation; they found a value to 19 kJ mol^{-1}. However, to determine the activity of M–NPs, the activation energy is a difficult parameter to interpret, so k is used as a comparison criterion. Table 1 shows the kinetic parameters obtained in this work and those reported in literature.

If we compare the k obtained for the reduction reaction catalyzed by our Au–NPs (1–3) with other catalytic systems, we can note that they are in an intermediate region. The values found for k indicate that they are less active in relation to Au–NPs stabilized with CTAB. However, 1–3 are two orders of magnitude more active than other systems based on supported Au–NPs. On the other hand, 1–3 have a catalytic activity about a thousand times higher than the Ag–NPs. We can note that only Pd–NPs have a considerably higher k than the rest of the catalytic systems. It is important to mention that, a variety of parameters have been reported in the literature in order to compare the activity between different catalytic systems. Most of these studies simply make use of the pseudo-first order rate constant (k_{obs} or k_{app}), without taking in consideration the catalyst loading. However, the determined value of TON (the number of moles of substrate/the number of moles of catalyst) for Au–NPs is around to 15 000.

Finally, it is important to mention that the synthesized nanoparticles not only showed an interesting catalytic effect in water even at room temperature, they can also be recovered and reused. Fig. 6 shows that after the first catalytic cycle there are

Table 1 Kinetic parameters in the reduction of DNB^a

M–NPs	Size (nm)	k (mol m^2 s^{-1})	Reference
1	9.0	13.41×10^{-3}	This work
2	15.0	2.79×10^{-3}	This work
3	15.0	46.83×10^{-3}	This work
Au–NPs^b	6.5	50.00×10^{-2}	40
Au–NPs^c	3.0	1.00×10^{-4}	31
Pd–NPs^d	4.0	1.51×10^{2}	41
Ag–NPs^e	2.5	1.00×10^{-4}	42

^{a} 25 °C. ^{b} Stabilized with CTAB. ^{c} Supported on polyelectrolytes. ^{d} On the surface of Fe_3O_4@dextrano. ^{e} Stabilized with exopolysaccharide.
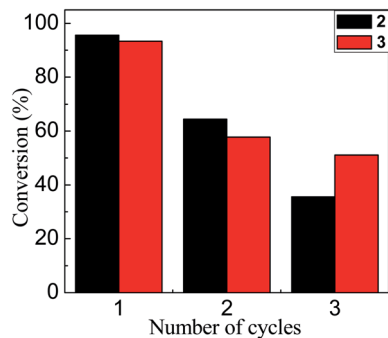
Fig. 6 Conversion rate based on the number of cycles in which 2 (black bars) and 3 (red bars) were catalytically active.

significant losses in the conversion. Two possible explanations for this observation are: (i) the loss of Au–NP in the catalyst recovery process in each cycle or, (ii) since the catalytic mechanism proposed is a process on the surface of Au–NPs, where the reagents compete for the free regions, the active sites can be occupied or modified after the reaction. Further work is in development in our laboratories focusing on the recovery process in each cycle of these water-soluble Au–NPs.

Experimental section

General

Tetrachloroauric acid ($HAuCl_4$, Sigma-Aldrich) as the precursor and hydrazine monohydrate ($N_2H_4 \cdot H_2O$, Sigma-Aldrich) as the reducing agent, both for the synthesis of Au–NPs were employed as received. The substrate 1,4-dinitrobenzene (DNB) from Sigma-Aldrich was employed as received. Ultrapure water was obtained from Labconco equipment model 90901-01. Imidazolium salts [1,3-bis(2,6-diisopropyl-4-sodiumsulfonatophenyl) imidazolium, 1-mesityl-3-(3-sulfonatopropyl)imidazolium and 1-(3-sulfonatopropyl)imidazolium] were prepared and characterized according to reported procedures.[43,44]

Synthesis of water-soluble Au–NPs

A stock solution of metal precursor ($[HAuCl_4] = 0.06$ M) was prepared in acetonitrile (Sintorgan HPLC quality). Following, an appropriate amount of this solution -to obtain a given concentration (1×10^{-4} M) of the metal precursor-was transferred to a volumetric flask, and the acetonitrile was evaporated by bubbling dry N_2; then, 1×10^{-4} M aqueous solution of sulfonated-imidazolium salt was added. Hydrazine was dissolved in the same aqueous solution. Hydrazine (Hz) concentration was 1×10^{-3} M when mixed (without stirring) with the metal precursor solution. The time course of the reaction was 3 seconds. Then, when the Au–NPs (1–3) were formed, the suspensions turned pink along the time.[25,26]

Catalytic experiments in water

The reactions were followed measuring the increase at the maximum absorption band of the p-nitroaniline (p-NA) at $\lambda_{max} = 380$ nm ($\varepsilon = 10\ 427$ M^{-1} cm^{-1}) at different temperature, $T_1 = 25.0 \pm 0.1$ °C, $T_2 = 35.0 \pm 0.1$ °C and, $T_3 = 45.0 \pm 0.1$ °C. Absorbance values at different times, were recorded in a Hewlett–Packard, UV-visible 8453 spectrophotometer equipped with a thermostated cell (3 mL of volume and 1 cm path length).

The UV-visible spectroscopic analysis (Scheme 2) shows that the reduction of DNB catalyzed by Au–NPs in water, produces p-NA in quantitative yields.

To start a kinetic run, 0.1 M solution of hydrazine in water was prepared in presence of Au–NPs, [Au–NPs] = 1×10^{-8} M. In a thermostated cell that contained the hydrazine and Au–NPs solutions, the reduction reactions were initiated by addition of different μL of the stock solution of DNB in order to have 3 mL of solution with the desired [DNB] concentrations. DNB concentration in water between 1.5×10^{-5} M to 1.5×10^{-4} M was varied.

Recover of Au–NPs

After the reaction is concluded, the Au–NPs are removed from the reactions medium by centrifugations for 25 min at 13.000 RPM and washed with pure water. Then, Au–NPs are suspended with 3 mL of water and sonicated for 5 min. The surface plasmon resonance (SPR) of Au–NPs was checked by UV-visible. In addition, the complete removal of the substrate (DNB) was confirmed by UV spectroscopy. Finally, to start other catalytic
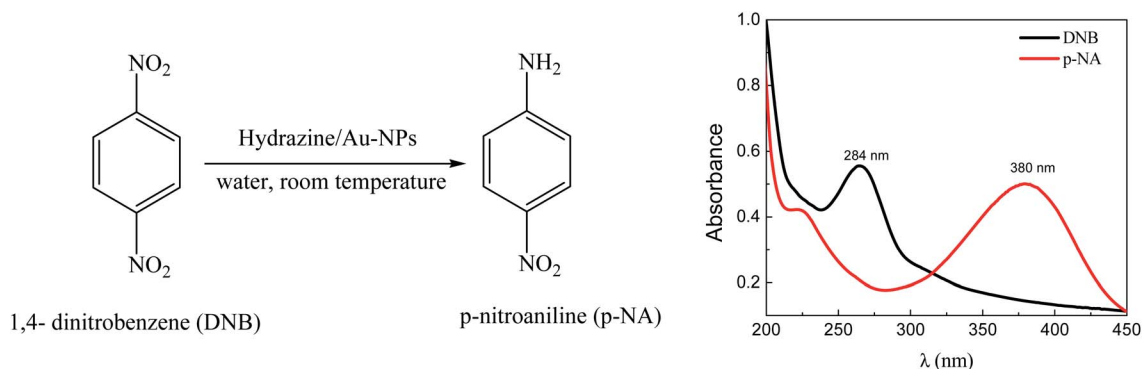
Scheme 2 Reduction of DNB using Au–NPs (1–3) as a catalyst and representative absorption spectra of the reactive (black line) and product (red line) in water.

reaction cycle, the desired amount of substrate is added from the stock solution.

Langmuir–Hinshelwood (LH) model

To quantify the catalytic reduction of 1,4-dinitrobenzene reaction, the well-known equations of Langmuir–Hinshelwood were applied.[31] It is an idealized model of bimolecular surface-mediated reactions and, involves certain considerable limitations in its application to real systems; nevertheless, it deserves some attention because this model is the basis for studying many reactions. The model assumes a uniform solid surface with no interaction between adsorbed species and, that the product of reaction is not absorbed on surface. In the LH model, the apparent kinetic rate constant, k_{app}, is strictly proportional to the total surface of nanoparticles (S) and the concentration of Hz. The, this can be defined through (eqn (3)).[31,37]

$$-\frac{dc_{DNB}}{dt} = kSc_{DNB}c_{HZ} = k_{app}c_{DNB} \quad (3)$$

where c_{DNB} and c_{HZ} is the concentrations of DNB and Hz, respectively at time t and, S is the total surface area of Au–NPs per unit volume of the solution. As the diffusion of the reagents and the adsorption–desorption steps are fast, the rate of the bimolecular reaction on the surface is proportional to the product of the fractions of the surface covered by the two reacting species so, we can rewrite the eqn (3) as:

$$\frac{dc_{DNB}}{dt} = -kS\,\theta_{DNB}\theta_{Hz} \quad (4)$$

where θ_{DNB} and θ_{Hz} are fractions of surface sites occupied by DNB and Hz, respectively. The k is the bimolecular rate constant and can be obtained from the kinetics analysis. The reactants, DNB and Hz, follow the Langmuir isotherm:[37]

$$\theta_{DNB} = \frac{(K_{DNB}c_{DNB})^n}{1 + (K_{DNB}c_{DNB})^n + (K_{Hz}c_{Hz})^m} \quad (4a)$$

$$\theta_{Hz} = \frac{(K_{Hz}c_{Hz})^m}{1 + (K_{DNB}c_{DNB})^n + (K_{Hz}c_{Hz})^m} \quad (4b)$$

Here, K_{DNB} and K_{Hz} are the adsorption coefficients of DNB and Hz, respectively, and c_{DNB} and c_{Hz} symbolize the respective concentrations in solution. The exponent n and m are related to the heterogeneity of the solid surface of the NPs. In others words, DNB and Hz may occupy adsorption sites on the surface of different energies.[31,37] Taking into account eqn (3) and (4a), eqn (5) and (6) can be obtained:

$$-\frac{dc_{DNB}}{dt} = \frac{kS(K_{DNB}c_{DNB})^n(K_{Hz}c_{Hz})^m}{(1 + (K_{DNB}c_{DNB})^n + (K_{Hz}c_{Hz})^m)^2} = k_{app}c_{DNB} \quad (5)$$

$$k_{app} = \frac{kSK_{DNB}{}^n c_{DNB}{}^{n-1}(K_{Hz}c_{Hz})^m}{(1 + (K_{DNB}c_{NB})^n + (K_{Hz}c_{Hz})^m)^2} \quad (6)$$

Eqn (6) allows to make the relation between the k_{app} values determined experimentally with the bimolecular rate constant values for each Au–NPs in solution, k. The S value of each Au–NPs can be calculated considering the analytical concentration,

Table 2 Catalyst parameters of the different Au–NPs used

	1	**2**	**3**
Analytical concentration[a] (M)	1×10^{-8}	1×10^{-8}	1×10^{-8}
Size[b] (nm)	9	15	13
Morphology	Spherical	Spherical	Spherical
Degree of surface coverage of the Au–NPs[c] (%)	59	67	48
Total surface area of the catalyst (m²)	3.03×10^{-4}	8.43×10^{-4}	6.33×10^{-4}

[a] Molar concentration of the Au–NPs solutions were calculated by dividing the total number of gold atoms over the average number of gold atoms per Au–NP.[35] [b] Diameters determined by TEM. [c] Obtained by TGA analysis.

the size, the morphologic and, the degree of surface coverage of the Au–NPs incorporated into the reaction medium. These values have been determined in our research group and due reported[26] (summarized in Table 2).

Conclusion

Three new water-soluble Au–NP (**1–3**) synthesized in our laboratory, proved to be an excellent active catalysts for the reduction of 1,4-dinitrobenzene at room temperature in water. In all cases, there is an induction time, and the activation energy found is suitable for restructuring at the surface of Au–NP, being consistent with other metal nanoparticles used for this reaction. Not least, all the nanoparticles were reusable in water for 3 cycles, using a quick, easy, economical and non-polluting method.

Conflicts of interest

There are no conflicts to declare.

Acknowledgements

References

1 A. S. K. Hashmi and F. D. Toste, *Modern Gold Catalyzed Synthesis*, 2012.
2 F. D. Toste and V. Michelet, in *Gold Catalysis*, Imperial College Press, 2011, vol. 13, pp. i–xvii.

3 M. Pan, J. Yang, K. Liu, Z. Yin, T. Ma, S. Liu, L. Xu and S. Wang, *Nanomaterials*, 2020, **10**, 209.

4 W. Guo, J. J. Li, Y. A. Wang and X. Peng, *Chem. Mater.*, 2003, **15**, 3125–3133.

5 K. Saha, S. S. Agasti, C. Kim, X. Li and V. M. Rotello, *Chem. Rev.*, 2012, **112**, 2739–2779.

6 T. Wang, S. Zhou, C. Zhang, J. Lian, Y. Liang and W. Yuan, *New J. Chem.*, 2014, **38**, 46–49.

7 V. G. Kravets, A. V. Kabashin, W. L. Barnes and A. N. Grigorenko, *Chem. Rev.*, 2018, **118**, 5912–5951.

8 P. Poizot, S. Laruelle, S. Grugeon, L. Dupont and J.-M. Tarascon, *Nature*, 2000, **407**, 496–499.

9 L. Armelao, S. Quici, F. Barigelletti, G. Accorsi, G. Bottaro, M. Cavazzini and E. Tondello, *Coord. Chem. Rev.*, 2010, **254**, 487–505.

10 S. Navalon, A. Dhakshinamoorthy, M. Alvaro and H. Garcia, *Coord. Chem. Rev.*, 2016, **312**, 99–148.

11 J. M. Walker and J. M. Zaleski, *Nanoscale*, 2016, **8**, 1535–1544.

12 P. Zhao, X. Feng, D. Huang, G. Yang and D. Astruc, *Coord. Chem. Rev.*, 2015, **287**, 114–136.

13 M. Tamura and H. Fujihara, *J. Am. Chem. Soc.*, 2003, **125**, 15742–15743.

14 M. V. Vasylyev, G. Maayan, Y. Hovav, A. Haimov and R. Neumann, *Org. Lett.*, 2006, **8**, 5445–5448.

15 C. Vollmer and C. Janiak, *Coord. Chem. Rev.*, 2011, **255**, 2039–2057.

16 N. Yan, C. Xiao and Y. Kou, *Coord. Chem. Rev.*, 2010, **254**, 1179–1218.

17 E. Guyonnet Bilé, R. Sassine, A. Denicourt-Nowicki, F. Launay and A. Roucoux, *Dalton Trans.*, 2011, **40**, 6524–6531.

18 S. Wegner and C. Janiak, in *Ionic Liquids II*, ed. B. Kirchner and E. Perlt, Springer International Publishing, Cham, 2017, pp. 153–184.

19 E. C. Hurst, K. Wilson, I. J. S. Fairlamb and V. Chechik, *New J. Chem.*, 2009, **33**, 1837–1840.

20 J. Vignolle and T. D. Tilley, *Chem. Commun.*, 2009, 7230–7232.

21 X. Ling, N. Schaeffer, S. Roland and M.-P. Pileni, *Langmuir*, 2013, **29**, 12647–12656.

22 A. Ferry, K. Schaepe, P. Tegeder, C. Richter, K. M. Chepiga, B. J. Ravoo and F. Glorius, *ACS Catal.*, 2015, **5**, 5414–5420.

23 E. A. Baquero, S. Tricard, J. C. Flores, E. de Jesús and B. Chaudret, *Angew. Chem., Int. Ed.*, 2014, **53**, 13220–13224.

24 B. S. Souza, E. C. Leopoldino, D. W. Tondo, J. Dupont and F. Nome, *Langmuir*, 2012, **28**, 833–840.

25 G. A. Monti, G. A. Fernández, N. M. Correa, R. D. Falcone, F. Moyano and G. F. Silbestri, *R. Soc. Open Sci.*, 2017, **4**, 1–7.

26 G. A. Monti, N. M. Correa, R. D. Falcone, G. F. Silbestri and F. Moyano, *ChemistrySelect*, 2019, **4**, 13496–13502.

27 P. Hervés, M. Pérez-Lorenzo, L. M. Liz-Marzán, J. Dzubiella, Y. Lu and M. Ballauff, *Chem. Soc. Rev.*, 2012, **41**, 5577–5587.

28 N. Pradhan, A. Pal and T. Pal, *Colloids Surf., A*, 2002, **196**, 247–257.

29 K. Esumi, R. Isono and T. Yoshimura, *Langmuir*, 2004, **20**, 237–243.

30 A. Grirrane, A. Corma and H. Garcia, *Nat. Protoc.*, 2010, **5**, 429–438.

31 S. Wunder, F. Polzer, Y. Lu, Y. Mei and M. Ballauff, *J. Phys. Chem. C*, 2010, **114**, 8814–8820.

32 S. Sarkar, A. K. Sinha, M. Pradhan, M. Basu, Y. Negishi and T. Pal, *J. Phys. Chem. C*, 2011, **115**, 1659–1673.

33 J. Zeng, Q. Zhang, J. Chen and Y. Xia, *Nano Lett.*, 2010, **10**, 30–35.

34 M. Nasrollahzadeh, M. Maham and S. Mohammad Sajadi, *J. Colloid Interface Sci.*, 2015, **455**, 245–253.

35 S. Wunder, Y. Lu, M. Albrecht and M. Ballauff, *ACS Catal.*, 2011, **1**, 908–916.

36 M. Nemanashi and R. Meijboom, *J. Colloid Interface Sci.*, 2013, **389**, 260–267.

37 S. Gu, S. Wunder, Y. Lu, M. Ballauff, R. Fenger, K. Rademann, B. Jaquet and A. Zaccone, *J. Phys. Chem. C*, 2014, **118**, 18618–18625.

38 Note: number of imidazolium salt per mn^2 for: **2** is 189 while for **3** is 121 according.

39 N. Lee, D.-W. Lee and S.-M. Lee, *Biomacromolecules*, 2018, **19**, 4534–4541.

40 R. Fenger, E. Fertitta, H. Kirmse, A. F. Thünemann and K. Rademann, *Phys. Chem. Chem. Phys.*, 2012, **14**, 9343–9349.

41 L. R. S. Lara, A. D. Zottis, W. C. Elias, D. Faggion, C. E. Maduro de Campos, J. J. S. Acuña and J. B. Domingos, *RSC Adv.*, 2015, **5**, 8289–8296.

42 Z. Zheng, Q. Huang, H. Guan and S. Liu, *RSC Adv.*, 2015, **5**, 69790–69799.

43 G. A. Fernández, A. B. Chopa and G. F. Silbestri, *Catal. Sci. Technol.*, 2016, **6**, 1921–1929.

44 C. Fleckenstein, S. Roy, S. Leuthäußer and H. Plenio, *Chem. Commun.*, 2007, 2870–2872.